JOURNAL OF COMPUTATIONAL PHYSICS 117, 28–34 (1995)

An Adaptive Discontinuous Finite Element Method for the Transport Equation

JENS LANG* AND ARTUR WALTER

Konrad Zuse Zentrum für Informationstechnik Berlin, Heilbronner Strasse 10, D-10711, Berlin-Wilmersdorf, Germany

Received July 31, 1992; revised July 18, 1994

In this paper we introduce a discontinuous finite element method. In our approach, it is possible to combine the advantages of finite element and finite difference methods. The main ingredients are numerical flux approximation and local orthogonal basis functions. The scheme is defined on arbitrary triangulations and two different error indicators are derived. Especially the second one is closely connected to our approach and able to handle arbitrary varying flow directions. Numerical resuls are given for boundary value problems in two dimensions. They demonstrate the performance of the scheme, combined with the two error indicators. © 1995 Academic Press, Inc.

1. INTRODUCTION

The transport equation arises in many areas of physics, such as reactor analysis, induction of electrons in solids, and the propagation of photons in stellar and planetary atmospheres. All these applications lead to equations of the form

$$\begin{aligned} \beta \cdot \nabla u(x,\beta) + \sigma(x)u(x,\beta) &= \int_{S^2} \alpha(x,\beta,\eta)u(x,\eta)\,d\eta \\ &\quad + f(x,\beta) \quad \text{for } x \in \Omega \qquad (1.1) \\ u(x,\beta) &= 0 \qquad \text{for } x \in \Gamma_-, \end{aligned}$$

where α is the transfer kernel describing the distribution of particles arising from scattering, fission, and capturing events, σ is the total cross section, and $S^2 := \{x \in \mathbb{R}^2 : |x| \le 1\}$. Further, Ω is in general a domain in $\mathbb{R}^3$ and $\Gamma_- := \{x \in \partial\Omega : \beta \cdot n(x) < 0\}$ its inflow boundary, with $n(x)$ denoting the outer unit normal to Ω at x. The unknown function $u = u(x, \beta)$ is the density of particles, moving in the direction β.

The numerical approach is to approximate the integral in (1.1) by a sum, using an angular quadrature scheme with N evaluation points. So we have to solve N transport equations of the form introduced in Section 2. Therefore, one should use an adaptive high resolution scheme for solving these transport equations to obtain a fast and accurate algorithm. These demands can be satisfied by a discontinuous finite element method, DFEM. This method is based on a local approach, which means that the solution is allowed to be discontinuous across interelement boundaries. The DFEM is already widely used for equations of the form (1.1). It was analyzed first by Lesaint and Raviart [8] and more recently by Johnson and Pitkäranta [7], who obtained improved error estimates. Later, Richter [11] developed a new approach to DFEM by using two types of triangles in his analysis. In a note on convergence Peterson [9] proved optimality of these error estimates for quasi-uniform meshes.

Our work was mainly stimulated by the paper of Cockburn *et al.* [3] in which nonoscillating finite difference methods are used in combination with finite element methods. To obtain physically relevant solutions of initial–boundary value problems associated with hyperbolic conservation laws, they proposed a special local projection, which does not destroy the high-order accuracy of their scheme. In contrast to those, our objective is to solve stationary convection–diffusion equations occurring in the context of (1.1). Nevertheless, we can use their finite element discretization combined with a numerical flux approximation. Additionally, an effective adaptation of the triangulation is taken into consideration, better resolving the local structures of such kinds of problems. Not only does it drastically reduce the number of degrees of freedom, but also it permits us to estimate the reliability of the solution by the computed error bounds.

Our variant of DFEM is characterized by the fact that we can involve the above-mentioned ideas while keeping the nice features of finite element methods, such as easy handling of complex geometries and boundary conditions. We can increase the accuracy locally rather than using wider stencils as in finite difference methods. Another important aspect of this approach is the possibility of transmitting the well established finite difference methodology for these equations to irregular grids and higher dimensions. The method is explicit, so no large linear systems need to be solved, and it is able to work on very irregular grids. This is necessary, since during the solution process the grid will be adapted to the solution.

Two error indicators are derived and compared. The first uses a dual problem in a standard way. The second is based on the ease of increasing *locally* the degree of the approximating

* Email: lang@sc.zib-berlin.de.

0021-9991/95 $6.00

polynomials in the context of DFEM. For this, we choose a basis of orthogonal polynomials on each triangle. Therefore, we can split the solution into its constant and linear parts. The magnitude of the linear part is taken as an error indicator. These motivations are reflected in the quite different behavior of the indicators in our applications.

The outline of the paper is as follows. In the second section we introduce the model equation and our scheme. It is shown that it fits well between finite difference and finite element methods. In the third section an error estimation is given in the case of a constant flow field vector β. For an arbitrary vector β we introduce the idea of local orthogonal basis functions and the corresponding error indicator. The last section includes some numerical experiments that are merely done to show the performance of the different indicators and for comparison with published calculations, e.g., [11]. Finally, a conclusion and some remarks on the discretization of convection–diffusion equations are given.

2. THE SCALAR LINEAR TRANSPORT EQUATION AND THE DERIVATION OF THE SCHEME

We consider the first-order hyperbolic equation

$$\begin{aligned} \beta \cdot \nabla u + \sigma u &= f \quad \text{in } \Omega, \\ u &= g \quad \text{on } \Gamma_-. \end{aligned} \tag{2.1}$$

as a model of Eq. (1.1). Here, Ω is a bounded polygonal domain in $\mathbb{R}^2$. The flow field vector $\beta : \Omega \to \mathbb{R}^2$ is a prescribed smooth vector field, σ is a bounded measurable function on Ω, f is in $L_2(\Omega)$, and g, the given inflow condition, is in $L_2(\Gamma_-)$.

Let $T_h = \{T\}$ be a quasi-uniform partition of the domain Ω into triangular elements T, which means that all angles of $T \in T_h$ are bounded from below by a positive constant. We denote by $P_\kappa(T)$ the space of polynomials of degree $\leq \kappa$ on $T \in T_h$. The DFEM for (2.1) is derived from the weak formulation on each $T \in T_h$. We replace the exact solution u by its possibly discontinuous approximation u_h with $u_h|_T \in P_\kappa(T)$. Finally, integration by parts yields for $v_h|_T \in P_\kappa(T)$

$$\begin{aligned} &\int_T u_h(-\nabla \cdot (\beta v_h) + \sigma v_h)\, dx + \int_{\partial T} u_h v_h \beta \cdot n\, ds \\ &\quad = \int_T f v_h\, dx. \end{aligned} \tag{2.2}$$

Since u_h is a discontinuous piecewise polynomial of degree κ over the triangulation T_h it is not defined exactly on ∂T. There are many possible choices for these variables at the boundaries. In the following we will use this indeterminacy to adopt the successful nonoscillatory methodology, see, e.g., [6], from the finite difference method. To this end we replace the flux function $u_h \beta \cdot n$ by some numerical average flux $h(u_h^{\text{int}}, u_h^{\text{ext}})$. With the following definitions for an $x \in \partial T$,

$$\begin{aligned} u_h^{\text{int}} &:= \lim_{x^i \to x} u_h(x^i) \quad \text{for } x^i \in \text{interior of } T \\ u_h^{\text{ext}} &:= \lim_{x^i \to x} u_h(x^i) \quad \text{for } x^i \in \text{exterior of } T, \end{aligned}$$

we can use a Lipschitz continuous "monotone" flux as given in [3]. There, Cockburn and his co-workers first proposed this idea for the solution of hyperbolic conservation laws in connection with the FEM. In the special case $\sigma = \nabla \cdot \beta$ we get exactly the steady state version of their scheme taken without any local projection of the solution. The function $h(\cdot, \cdot)$ satisfies the consistency relation $h(u, u) = u\beta \cdot n$, is nondecreasing in its first argument, and is nonincreasing in its second argument. Scheme (2.2) now reads:

For given $u_h^{\text{ext}} = g$ on Γ_-, find $u_h|_T \in P_\kappa(T)$, such that for each triangle $T \in T_h$,

$$\begin{aligned} &\int_T u_h(-\nabla \cdot (\beta v_h) + \sigma v_h)\, dx + \int_{\partial T} h(u_h^{\text{int}}, u_h^{\text{ext}}) v_h\, ds \\ &\quad = \int_T f v_h\, dx, \forall v_h \in P_\kappa(T). \end{aligned} \tag{2.3}$$

A possible choice for $h(\cdot, \cdot)$ is the Engquist–Osher two-point monotone flux, which for an arbitrary function $\text{fl}(u)$ is defined by

$$\begin{aligned} h^{\text{EO}}(a, b) := &\int_0^b \min(fl'(s), 0)\, ds \\ &+ \int_0^a \max(\text{fl}'(s), 0)\, ds + \text{fl}(0). \end{aligned} \tag{2.4}$$

The next result gives an interesting connection to the DFEM introduced by Reed and Hill [10]. First, we recall their formulation of the method: For given $u_h^- = g$ on Γ_-, find $u_h|_T \in P_\kappa(T)$ such that for each $T \in T_h$

$$\begin{aligned} &\int_T (\beta \cdot \nabla u_h + \sigma u_h) v_h\, dx + \int_{\partial T_-} (u_h^+ - u_h^-) v_h |\beta \cdot n| ds \\ &\quad = \int_T f v_h\, dx, \quad \forall v_h \in P_\kappa(T), \end{aligned} \tag{2.5}$$

with $\partial T_- = \{x \in \partial T : \beta \cdot n(x) < 0\}$ and $u_h^\pm = \lim_{\varepsilon \to 0^\pm} u_h(x + \varepsilon\beta)$.

LEMMA 2.1. *The method* (2.5) *is equivalent to* (2.3) *with the numerical flux approximation* (2.4).

Proof. Using

$$\begin{aligned} \int_{\partial T} h^{\text{EO}}(u_h^{\text{int}}, u_h^{\text{ext}}) v_h\, ds = &\int_{\partial T} (u_h^{\text{ext}} \min(\beta \cdot n, 0) \\ &+ u_h^{\text{int}} \max(\beta \cdot n, 0)) v_h\, ds \end{aligned}$$

$$= \int_{\partial T_+} u_h^{\text{int}} v_h |\beta \cdot n| ds - \int_{\partial T_-} u_h^{\text{ext}} v_h |\beta \cdot n| ds,$$

with $\partial T_+ = \{x \in \partial T : \beta \cdot n(x) \geq 0\}$ and the reformulations

$$u_h^{\text{int}}|_{\partial T_+} = u_h^-, \quad u_h^{\text{ext}}|_{\partial T_-} = u_h^-$$

the lemma follows from integration by parts of the left-hand side of (2.3). ∎

Remark 2.2. With the above lemma 2.1, the DFEM, as analyzed in [7], is a special case of the generalized discontinuous Galerkin method (2.3). An important aspect of this approach is its ability to generalize the well-established finite difference schemes to very irregular grids.

Remark 2.3. Unfortunately, the DFEM loses accuracy in a fairly large region near steep fronts of the solution, due to oscillations in the approximation. To overcome this difficulty the values of u_h^{ext}, u_h^{int} in (2.3) must be limited or computed with an adaptive stencil. In the finite difference theory of the last 10 years numerical methods like ENO (essentially nonoscillatory) or MUSCL (monotone upstream schemes for conservation laws) schemes were developed, which suppress such oscillations very successfully. Our numerical experiments in Section 4 have shown that (2.5) is not monotone. The remedy proposed by us for our simple numerical flux is to adapt the grid. To this end, the error indicators in Section 3 are developed.

It has been shown in [8] that for constant β an ordering of the triangles $\{T_1, T_2, \ldots\}$ exists, such that the finite element approximation can be computed in an explicit way. The same was done in [5] for $|\beta \cdot n| > 0$ for all sides of the triangles in T_h. The ordering is also possible if $\operatorname{div}(\beta) = 0$; see [13]. With such an ordering of the triangles it is possible to compute u_h successively on each $T \in T_h$, starting at the inflow boundary Γ_- where $u_h^- = g$ is given. For these cases, transport problems like (2.1) are connected to explicit methods in a natural way.

For further analysis, we introduce for each triangle T a finite element space V_h defined by

$$V_h := \{v_h \in L_2(\Omega) : v_h|_T \in P_\kappa(T),\ T \in T_h\}.$$

Note that any choice of the degree of freedom of the approximate solution is allowed in this formulation; cf. [5]. Summing over all $T \in T_h$ in (2.3), we arrive at the following equivalent formulation of (2.3): Find $u_h \in V_h$ such that

$$B(u_h, v_h) = (f, v_h), \quad \forall v_h \in V_h, \tag{2.6}$$

where

$$B(w, v) := \sum_{T \in T_h} \{(w, -\nabla \cdot (\beta v) + \sigma v)_T + (h, v)_{\partial T}\}. \tag{2.7}$$

Here $(\cdot, \cdot)_T$, $(\cdot, \cdot)_{\partial T}$ denote the $L_2(T)$, $L_2(\partial T)$ inner products. In the special case $h = h^{\text{EO}}$ we get

$$B(w, v) = B_1(w, v) - \int_{\Gamma_-} g v^+ |\beta \cdot n| \, ds \tag{2.8}$$

with

$$\begin{aligned} B_1(w, v) &:= \sum_{T \in T_h} \int_T w(-\nabla \cdot (\beta v) + \sigma v) \, dx \\ &\quad + \int_{\Gamma_h} w^-(v^- - v^+)|\beta \cdot n| \, ds + \int_{\Gamma_+} w^- v^- |\beta \cdot n| \, ds \end{aligned} \tag{2.9}$$

and $\Gamma_+ = \{x \in \partial\Omega : \beta \cdot n > 0\}$; cf. [7]. All the interelement boundaries are denoted by $\Gamma_h := \left(\bigcup_{T \in T_h} \partial T\right) \backslash \partial\Omega$. Of course, we can replace u_h by the exact solution u in (2.6); i.e., we have the consistency relation

$$B_1(u - u_h, v_h) = 0, \quad v_h \in V_h. \tag{2.10}$$

3. ERROR ESTIMATES

3.1. *Constant Unit Flow Field Vector* β

For constant unit β Johnson and Pitkäranta [7] obtained for the DFEM (2.5) various stability and convergence results, including an L_2-error estimate of the form

$$\|u - u_h\|_{0,\Omega} \leq C \cdot h^{\kappa + 1/2} |u|_{\kappa+1,\Omega}. \tag{3.1}$$

This error estimate is based on the stability inequality

$$|u_h|_{h,\beta} + \|u_h\|_{0,\Omega} \leq C(\|f\|_{0,\Omega} + \|g\|_{0,\Gamma_-}), \tag{3.2}$$

where $|\cdot|_{h,\beta}$ is a mesh-dependent seminorm which controls the derivative $\beta \cdot \nabla u_h$ and the jumps of $u_h \beta \cdot n$ across the interelement boundaries. This stability result is, of course, also true for (2.3), (2.4). In what follows, we will present another proof of the convergence result (3.1), using only a special part of $|\cdot|_{h,\beta}$,

$$\|(u_h^+ - u_h^-)|\beta \cdot n|^{1/2}\|_{0,\Gamma_h} + \|u_h^+ |\beta \cdot n|^{1/2}\|_{0,\Gamma} \leq |u_h|_{h,\beta}. \tag{3.3}$$

We start our derivation by considering the dual problem to (2.1),

$$\begin{aligned} -\beta \cdot \nabla \varphi + \sigma \varphi &= \Theta \quad \text{in } \Omega, \\ \varphi &= 0 \quad \text{on } \Gamma_+, \end{aligned} \tag{3.4}$$

with $\Theta \in L_1(\Omega)$. In the next step we seek an approximate solution $\varphi_h \in V_h$ such that

$$B_1(v_h, \varphi_h) = (\Theta, v_h), \quad v_h \in V_h, \tag{3.5}$$

where B_1 is as in (2.9). The function φ_h is the discontinuous Galerkin solution of (3.4). Now, we introduce the local L_2-projection $\tilde{u} \in V_h$ of the exact solution u by

$$\int_T (u - \tilde{u})v \, dx = 0, \quad v \in P_\kappa(T), T \in T_h. \tag{3.6}$$

Applying the Bramble–Hilbert lemma [2] and a standard estimate of norms over boundaries, see, e.g., [1], we get

$$\|u - \tilde{u}\|_{0,T} \leq Ch^{\kappa+1}|u|_{\kappa+1,T},$$
$$\|u - \tilde{u}\|_{0,\partial T} \leq Ch^{\kappa+1/2}|u|_{\kappa+1,T}.$$

With the choice $\Theta = v_h = (u_h - \tilde{u}) \in V_h$ and recalling (2.10),

$$\begin{aligned}\|u_h - \tilde{u}\|_{0,\Omega}^2 = B_1(u - \tilde{u}, \varphi_h) &= (u - \tilde{u}, -\beta \cdot \nabla\varphi_h + \sigma\varphi_h) \\ &+ \int_{\Gamma_h} (u - \tilde{u})^-(\varphi_h^- - \varphi_h^+)|\beta \cdot n| \, ds \\ &+ \int_{\Gamma_+} (u - \tilde{u})^-\varphi_h^-|\beta \cdot n| \, ds.\end{aligned}$$

Since $\beta \cdot \nabla\varphi_h \in V_h$ the corresponding term is eliminated by (3.6). With the formal substitutions $u_h := \varphi$, $\beta := -\beta$, $\Gamma_- := \Gamma_+$, $f := \Theta$ and the setting $g = 0$, the stability result (3.2) remains true for the problem (3.4). It follows by the Cauchy–Schwarz inequality that

$$\|u_h - \tilde{u}\|_{0,\Omega} \leq (C_1h^{\kappa+1/2} + C_2\|\sigma\|_{\infty,\Omega}h^{\kappa+1})|u|_{\kappa+1,\Omega}.$$

Using the triangle inequality we finally obtain

$$\begin{aligned}\|u - u_h\|_{0,\Omega} &\leq \|u - \tilde{u}\|_{0,\Omega} + \|u_h - \tilde{u}\|_{0,\Omega} \\ &= (C_1h^{\kappa+1/2} + C_2(\|\sigma\|_{\infty,\Omega} + 1)h^{\kappa+1})|u|_{\kappa+1,\Omega}.\end{aligned} \tag{3.7}$$

This completes the proof. ∎

Remark 3.1. The rate of convergence guaranteed by result (3.7) is less than the optimal rate $\kappa + 1$ by $\frac{1}{2}$. Peterson [9] presented a numerical example which shows that this order cannot be improved within the class of quasi-uniform meshes, not even for smooth exact solution u. On the other hand, for a non-smooth solution u the above error estimate is useless; e.g., if u is discontinuous it may be that $\|u\|_1 = \infty$.

An obvious idea for improving u_h during an adaptive process is the equidistribution of all local element errors. To give (3.7) a practical meaning, an approximation $D_T^{\kappa+1}u_h$ of the Sobolev seminorm $|u|_{\kappa+1,T}$ is needed. This can be done by using the numerical solution u_h. We refer the interested reader to [4]. For a local error indicator we can use

$$\begin{aligned}\|u - u_h\|_{0,T} \approx C(&h^{\kappa+1/2} \\ &+ (\|\sigma\|_{\infty,T} + 1)h^{\kappa+1})D_T^{\kappa+1}u_h, \quad T \in T_h.\end{aligned} \tag{3.8}$$

3.2. *Arbitrary Flow Field Vector* β

The situation becomes more complicated if β is an arbitrary vector function, not necessarily constant or with vanishing divergence. In this case neither stability nor convergence results are known. Nevertheless, we can use the flexibility of our scheme and increase the degree of the approximating polynomials locally to derive an efficient error indicator. To achieve this, we have to choose the polynomials appropriately. Performing the adaptation of the grid in this way, we avoid the above-mentioned drawback of the DFEM.

For the implementation of (2.6) we use a *local orthogonal basis* in $P_\kappa(T)$, $\{v_0^T, v_1^T, ..., v_l^T\}$, $l \in \mathbb{N}$, such that v_i^T has support in T and

$$(v_i^T, v_j^T) = C_i\delta_{ij}, \quad C_i \neq 0, i, j = 0, 1, ..., l.$$

This orthogonality is achieved by choosing an orthogonal basis over the standard triangle $\Delta := \{(\xi, \eta) \in \mathbb{R}^2 : 0 \leq \xi, \eta \leq 1, \xi + \eta \leq 1\}$,

$$v_0^\Delta = 2, \quad v_1^\Delta = 6\xi - 2, \quad v_2^\Delta = 2\sqrt{6}(\xi + 2\eta - 1), \quad ....$$

For simplicity of presentation, we restrict ourselves to the case $\kappa = 1$, i.e., to linear polynomials. Using an affine–linear mapping $F : \Delta \to T \in T_h$, we get in this case

$$\begin{aligned}v_0^T &= \tfrac{1}{2}v_0^\Delta(\xi(x_1, x_2), \eta(x_1, x_2)) = 1, \\ v_i^T &= \sqrt{|T|}/2v_i^\Delta(\xi(x_1, x_2), \eta(x_1, x_2)), \quad i = 1, 2,\end{aligned} \tag{3.9}$$

where $|T|$ stands for the area of T. The choice of constants will become clear below. If we define the degrees of freedom as

$$u_T^{(m)} = \frac{1}{|T|^\gamma}\int_T uv_m^T \, dx, \quad T \in T_h, \quad m = 0, 1, 2, \tag{3.10}$$

with $\gamma = 1$ if $m = 0$ and $\gamma = 2$ if $m = 1, 2$, we get the approximation of the exact solution in V_h by

$$u_h(x) = \sum_{m=0}^{2} u_T^{(m)}v_m^T(x), \quad x \in T, T \in T_h. \tag{3.11}$$

We remark that $u_T^{(0)}$ is an approximation of the average of the exact solution u in T. Moreover, by our construction (3.9), the

basis functions v_i^T, $i = 1, 2$, vanish at the midpoint x^{mid} of the triangle T; i.e., for $\kappa = 1$,

$$u_h(x^{\text{mid}}) = u_T^{(0)}. \tag{3.12}$$

The discontinuous piecewise linear approximation u_h can be locally split into a linear part out of $S_1(T)$ and a constant part out of $P_0(T)$. From the orthogonality of these two parts, i.e., $P_1 = P_0 \oplus S_1$, it follows that the greater the local gradients of the solution u the greater the part in S_1 of the numerical approximation u_h. This part tells us how difficult it is to approximate the function u in the corresponding region. Indeed, assuming that the fully linear FE-approximation is better than the constant one, i.e.,

$$\|u - u_T^{(0)}\|_{0,T} > \|u - u_h\|_{0,T}, \tag{3.13}$$

it is reasonable to expect that

$$\begin{aligned} \|u - u_T^{(0)}\|_{0,T} &\sim \|u_h - u_T^{(0)}\|_{0,T} \\ &= \left\| \sum_{m=1}^{2} u_T^{(m)} v_m^T(x) \right\|_{0,T}, \quad T \in T_h. \end{aligned} \tag{3.14}$$

In other words, under the assumption (3.13), the solution part lying in S_1 can be used as an indicator of the size of the actual error $\|u - u_T^{(0)}\|_{0,T}$. Clearly, the derivation described above is applicable for arbitrary $l \in \mathbb{N}$, too.

Remark 3.2. Another motivation for the above proposed local error indicator was given by one of the reviewers. He noted that since u_h is locally affine, we have that, for (x, y) in the triangle T,

$$u_h(x, y) = u_T^{(0)} + (x - x_B, y - y_B) \cdot \nabla u_h,$$

where (x_B, y_B) is the barycenter of the triangle T. Thus, applying an inverse estimate for linear finite elements, we get

$$\|u_h - u_T^{(0)}\|_{0,T} \sim \|\nabla u_h\|_{L^1(T)} \sim \|\nabla u\|_{L^1(T)}.$$

This relation shows that the error indicator is able to realize such regions associated with high local variations of the solution u.

Since we are equipped with local error indicators δ_j, $j = 1, \ldots, n$, n = number of elements, the obvious idea is to improve the finite element solution to a given tolerance *eps* in an adaptive process through equidistribution of all element errors. We search for a refinement strategy,

$$\text{Refine } T_j \text{ if } \delta_j > \text{cut}.$$

In order to achieve this, we determine "cut" by

$$\text{cut} := \frac{c}{n} \sum_{j=1}^{n} \delta_j$$

with some constant c which guarantees a desirable rate of refinement. In practical computations 30–50% of the elements are usually refined.

4. NUMERICAL RESULTS

The numerical experiments are mainly done to demonstrate the different behavior of the two error indicators (3.8) and (3.14) and the high accuracy of the method. These are also documented by other authors, e.g., [11]. This makes a direct comparison of the results possible. To the first example, the transportation of a steep front along a straight line, both error indicators are applied. The behavior during the refinement process and the final grids, which are necessary to obtain a good approximation of the exact solution with our algorithm, are compared. The second example is a transportation of the inflow condition along circular lines around the origin. This problem is known in the literature as a very hard one, because the streamlines are bent and the distance between the inflow and the outflow boundaries is relatively long. The divergence of the corresponding flow field in both examples is zero, and the triangles can be ordered, obtaining an explicit algorithm.

4.1. *Example 1: Transportation along a Line*

The first problem we consider is Eq. (2.1) on $\Omega = (0; 1) \times (0; 1)$ with $\sigma = 0, f = 0$, and the flow direction $\beta = (1.0; 1.0)$. The inflow boundaries are the lines $\{(x, y) \in \mathbb{R}^2 : x = 0\}$ and $\{(x, y) \in \mathbb{R}^2 : y = 0\}$ with the boundary condition

$$g(x, y) := \begin{cases} 0 & \text{if } \frac{5}{64} \geq y \\ \exp\left(\dfrac{(x - \frac{1}{16})^2}{(x - \frac{1}{16})^2 - (\frac{1}{64})^2} \right) & \text{if } \frac{5}{64} > y > \frac{1}{16} \\ 1 & \text{else.} \end{cases}$$

Thus, the steep front in the boundary condition does not coincide with the initial grid lines. The calculations are done on the basis of the adaptive FEM program KASKADE implemented by [12]. It should be mentioned that in nearly all applications published, the grid lines are chosen to represent the "near-discontinuity" of $g(x, y)$ at the inflow boundary (see Fig. 1).

The first picture shows the intermediate grid, produced by the first error indicator, left, and the second indicator, right. They are applied in such a way that in each refinement step no more than $\frac{1}{4}$ of the coarser grid triangles are refined. It can be seen that both indicators try to resolve the inflow condition. The difference occurs at the outflow boundary. Through the explicit solution process, the flow field is calculated along β and the greatest amount of error is at the outflow part of $\partial\Omega$. The derivation of the first error indicator started from the adjoint

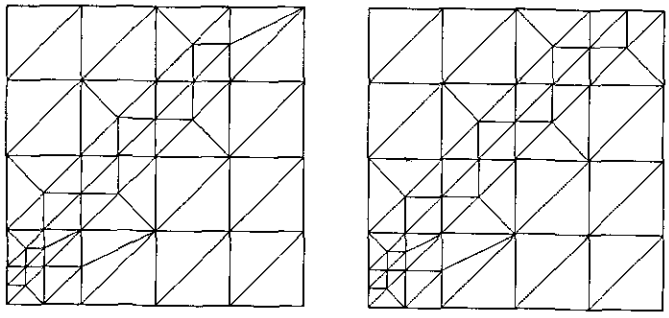

FIG. 1. Intermediate grids for Example 1.

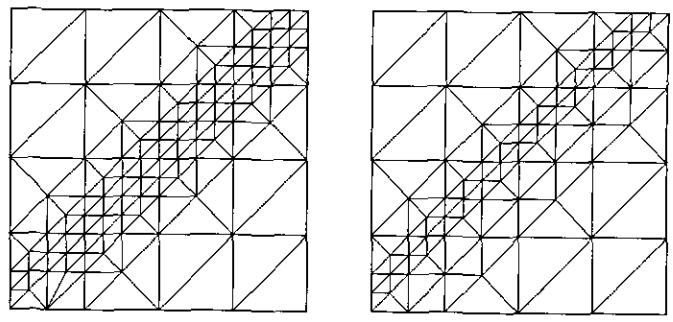

FIG. 3. Final grids.

problem (3.4) to (2.1); in particular β is replaced by $-\beta$, the opposite flow direction. So it takes this rough solution as a reference. This is also reflected by the solution after three refinement steps, which is shown in Fig. 2. The solution is plotted so that each triangle is colored with respect to $u_T^{(0)}$. We divided the range from -1 to 2 into 16 equidistant gray scales to include possible over- and undershoots. For each grid point we have as many solution values as triangles containing this point. The solution is neither interpolated nor smoothed to show the high resolution of the scheme. On the left grid, produced by indicator (3.8), the algorithm is not able to resolve the outflow in the same manner as on the grid generated by (3.14). In Fig. 3 the final grids after five refinement steps, which were necessary to resolve the critical line $y = x + \frac{1}{16}$, are shown. The left grid, corresponding to (3.8), is one refinement level deeper than the right one for the reasons discussed above.

4.2. *Example 2: Circulation of a Pulse*

In this case Eq. (2.1) is given on the domain $\Omega = \{(-1.0; 1.0) \times (-1.0; 1.0)\}\backslash\Gamma$ with the variable flow direction $\beta = (y, -x)$. Here $\sigma = 0$, $f = 0$, and the boundary condition on the inflow part is set to zero with the exception of $\Gamma := \{(x; y): x = 0 \wedge 0 \geq y \geq -1\}$. Here we use

$$g(y) := \begin{cases} 0 & \text{if } 0 \geq y > -0.1 \\ 1 & \text{if } -0.1 \geq y \geq -0.5 \\ 0 & \text{if } -0.5 > y \geq -1.0. \end{cases}$$

The exact solution is a transport of this "rectangular" inflow condition along circular lines around the origin to the outflow boundary, which is located opposite Γ. In this case, the indicator (3.8) has no theoretical justification, at least in our derivation, in Section 3. So it should not be applied here. These considerations are enforced by the numerical results.

Figure 4 shows the grid produced by (3.14) and the solution after six refinement steps. It can be seen that the algorithm begins to resolve the discontinuous solution starting from the inflow boundary along the streamlines. It is also interesting to see that the longer the streamlines are the more difficult it is to resolve the discontinuity. Figure 5 shows the final grid with about 8000 triangles, obtained after 12 refinements. The L_2 error is approximately 10% with an overshoot of 1.1 and an undershoot of -0.03. The time required to obtain this solution was about 8 min on a Sun Sparc-1 workstation. To compare this result, we mention [5]. There nearly 20,000 triangles are needed to follow a smooth inflow condition transported along grid lines on an equidistant grid. In spite of our remark on the error (3.8) made above, we tried it on the same problem since local smoothness is guaranteed. The result is shown in Fig. 6.

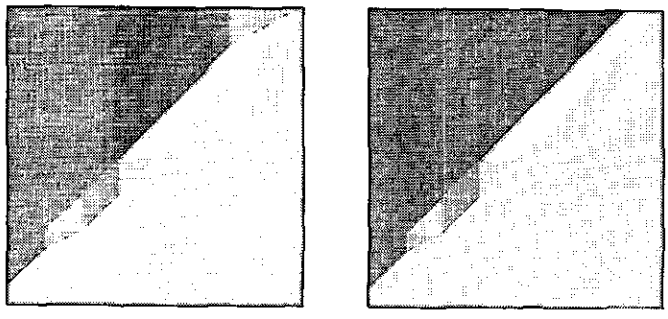

FIG. 2. Solution of Example 1 on intermediate grids.

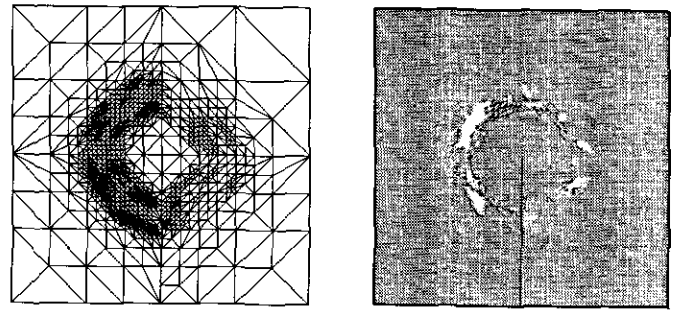

FIG. 4. Intermediate grid and solution for Example 2.

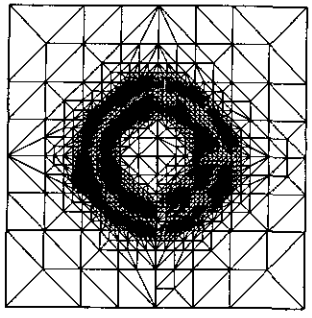

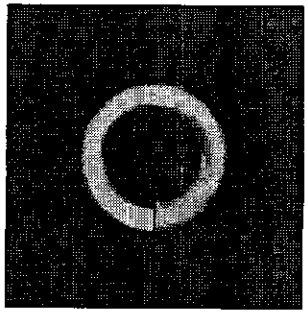

FIG. 5. Final grid and solution for Example 2.

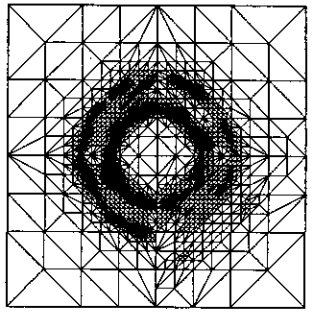

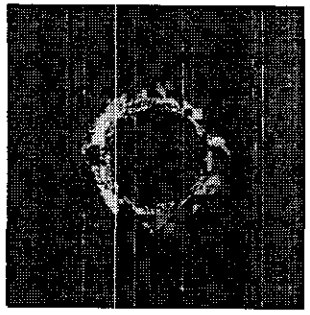

FIG. 6. Grid and solution for Example 2 with indicator (3.14).

The indicator was not able to adapt the grid along the streamlines. After four refinement steps all further refinement takes place near the inflow region of Ω. The grid consists of more than 10,000 triangles and gives an evidently worse solution than in Fig. 5.

5. CONCLUDING REMARKS

We have proposed a discontinuous finite element method for the transport equation. The method is of arbitrary order and can be applied in an explicit manner on quite irregular grids. Through its derivation the scheme can combine the nice features of finite element methods with successful techniques of finite difference schemes. Furthermore, it provides a very useful and robust error indicator. Our analysis and numerical results suggest that it can be used in a rather efficient manner in general situations.

One extension of the method should be to stationary convection-dominated convection–diffusion equations. In our approach, we approximate the solution by linear functions over each triangle. So we have to solve 3×3 linear systems locally. Since the solution is possibly discontinuous across interelement boundaries, the Laplacian operator cannot be discretized in a suitable manner. A remedy is to split the equation into two transport equations, as these are discretized by the mixed finite element method. However, this means that we have to solve 15×15 linear systems on each triangle—a significant increase in numerical work, which does not seem practical to us. This topic constitutes the subject of ongoing work.

ACKNOWLEDGMENTS

The authors thank R. Roitzsch for his patient support during the implementation of the algorithm. In addition, we wish to acknowledge the reviewers for their very constructive and helpful remarks leading to an improved version of the paper.

REFERENCES

1. R. A. Adams, *Sobolev Spaces* (Academic Press New York, 1975).
2. J. H. Bramble and S. R. Hilbert, *SIAM J. Numer. Anal.* **7,** 112 (1970).
3. B. Cockburn, S. Hou, and C.-W. Shu, *Math. Comp.* **54**(190), 545 (1990).
4. K. Erikson and C. Johnson, Technical report, Dept. of Mathematics, Chalmers Univ. of Technology, 1990 (unpublished).
5. R. S. Falk and G. R. Richter, *SIAM J. Numer. Anal.* **24**(2), 257 (1987).
6. A. Harten and S. Osher, *SIAM J. Numer. Anal.* **24**(2), 279 (1987).
7. C. Johnson and J. Pitkäranta, *Math. Comput.* **46**(173), 1 (1986).
8. P. Lesaint and P.-A. Raviart, "On a Finite Element Method for Solving the Neutron Transport Equation," in *Mathematical Aspects of Finite Elements in Partial Differential Equations*, edited by C. de Bour Academic Press, New York, (1974), p. 89.
9. T. E. Peterson, *SIAM J. Numer. Anal.* **28**(1), 133 (1991).
10. W. H. Reed and T. R. Hill, Technical Report LA-UR-73-479, Los Alamos National Laboratory, Los Alamos, NM, 1973 (unpublished).
11. G. R. Richter, *Math. Comp.* **50**(181), 75 (1988).
12. R. Roitzsch, Technical Report TR89-5, Konrad Zuse Zentrum für Informationstechnik Berlin, 1989 (unpublished).
13. R. Touzani, *Comput. Methods Appl. Mech. Eng.* **68,** 115 (1988).